

Non-imaging real-time detection and tracking of fast-moving objects using a single-pixel detector

Fengming Zhou

Abstract: Detection and tracking of fast-moving objects have widespread utility in many fields. However, fulfilling this demand for fast and efficient detecting and tracking using image-based techniques is problematic, owing to the complex calculations and limited data processing capabilities. To tackle this problem, we propose an image-free method to achieve real-time detection and tracking of fast-moving objects. It employs the Hadamard pattern to illuminate the fast-moving object by a spatial light modulator, in which the resulting light signal is collected by a single-pixel detector. The single-pixel measurement values are directly used to reconstruct the position information without image reconstruction. Furthermore, a new sampling method is used to optimize the pattern projection way for achieving an ultra-low sampling rate. Compared with the state-of-the-art methods, our approach is not only capable of handling real-time detection and tracking, but also it has a small amount of calculation and high efficiency. We experimentally demonstrate that the proposed method, using a 22kHz digital micro-mirror device, can implement a 105fps frame rate at a 1.28% sampling rate when tracks. Our method breaks through the traditional tracking ways, which can implement the object real-time tracking without image reconstruction.

Keywords: Hadamard pattern, single-pixel detector, real-time tracking, ultra-low sampling rate

1. Introduction

Real-time detection and tracking of fast-moving objects are widely used in scientific research, autonomous driving, industrial measurement, national defense security, bio-medicine and many other fields. Radar is an image-free target detection and tracking technology [1-4]. It emits electromagnetic waves at a certain frequency, and the electromagnetic waves are reflected when encountering an object and can be detected by the radar. With the development of various image sensors, image-based system [5-7] are more widely used as the price of sensors are cheaper.

The detection and imaging are two independent parts of the image-based fast-moving object tracking method. The moving objects need to be detected and tracked from continuous and clear images, and its accuracy depends on the quality of the captured image. The main factor affecting the image quality is motion blur caused by fast-moving targets. However, the equipment that constitutes a high time resolution imaging system is expensive, and the data throughput requires a large storage capacity and a wide data transmission bandwidth. Besides, the advanced image processing and analysis algorithms also take up a lot of computing resources. Gong W et al. [8-15] discussed high refresh rate and efficient reconstruction algorithms image-based moving target detection and tracking. However, these methods are not applicable when the target is moving too fast. Moreover, methods which obtains motion information through the evolution process of moving objects require high-precision tracking and aiming systems [16-18]. [19] points out the target tracking does not require a clear image, which the position information can be calculated from the relationship between rough images. Yet, this method relies on the imaging process that consumes a lot of computing time and memory. In summary, the complex image processing and

analysis algorithms and limited computing resources pose challenges to real-time target detection and tracking in practical applications.

In essence, detection and tracking of fast-moving objects only need to obtain their two-dimensional or three-dimensional spatial information. Compared with imaging that requires thousands of pixels, only two or three scalars are needed to determine the locations of the target, which reduces the amount of calculation by three to four orders of magnitude. In the image-based method, most of the captured image data is redundant, which is, it goes without saying, one of the main reasons hindering real-time target detection and tracking. To solve this problem, Shi et al. [20] proposed a method based on single-pixel imaging (SPI), using the "slice theory" of Hadamard transform to decompose the Hadamard matrix, which can track the target without obtaining a complete image. And an image-free method was recently proposed, based on Fourier single-pixel imaging (FSI), which allows real-time tracking of fast-moving objects [21].

Here, an image-free fast-moving objects real-time detection and tracking method based on Hadamard single-pixel imaging theory (HSI) is proposed, named PCGD. Using the HSI-based technology [22-26], we reconstruct the projection curves of a complex scene in the x-axis and y-axis direction without acquiring the scene image, in which the curves include location information. And then, we calculate the gradient difference of the projection curves to obtain the position information of the fast-moving target. In other words, the proposed method can convert the target scene from two-dimensional to one-dimensional, which reduce the amount of calculation and storage space occupation and significantly improves real-time performance.

Furthermore, a new sampling method based on contour moment technology, named EAHSI, is adopted to improve the efficiency of reconstructing projection curves. It optimizes the Hadamard pattern sequence, according to the size of the effective region (the white region of patterns), by sort the projection order. Consequently, a small number of patterns in the optimized sequence are used to measure large-amplitude coefficients and ignore the rest to improve efficiency [24,33-34]. The EAHSI only acquires the resulting light signal collected by a single-pixel detector for reconstructing the projection curves. Compared with the state-of-the-art methods, the EAHSI has the ability of ultra-low sampling rate, which is more suitable for real-time detection and tracking of fast-moving objects in the sampling stage.

2. Theory

2.1. Hadamard pattern construction and the principle of HSI

Hadamard single-pixel imaging (HSI) [27-29] is a new imaging technology. We can reconstruct images by spectrum after Hadamard transform, in which the spectrum consists of a set of Hadamard coefficients, each corresponding to a unique pattern. The pattern, a standard orthogonal basis, is formed by reshaping a row (or a column) of the Hadamard matrix into a two-dimensional square, as shown in Fig. 1. And it is a kind of square matrix whose elements are 1 or -1, whose rows (or columns) are orthogonal to each other.

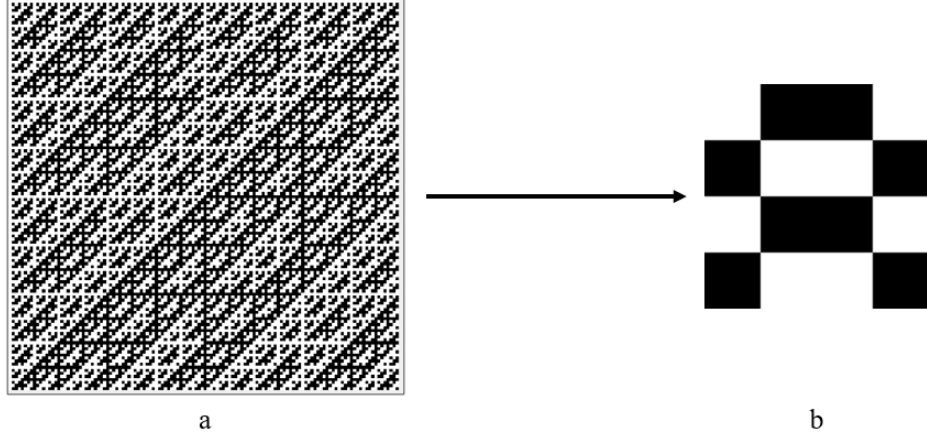


Fig. 1. The Hadamard pattern is obtained by reshaping the 4193rd row of the Hadamard matrix.

And the lowest order of Hadamard matrix is two, the higher order Hadamard matrix is obtained by formula $H_{2^{n+1}} = H_{2^n} \otimes H_2$, \otimes is the Kronecker product operator and H_2 is shown as Eq.1.

$$H_2 = \begin{bmatrix} 1 & 1 \\ 1 & -1 \end{bmatrix}. \quad (1)$$

The Hadamard coefficient can be obtained by projecting the pattern onto the object. It is mathematically equivalent to the inner product between the pattern and scene. So, we can calculate the Hadamard spectrum by using the measurement values collected by a single-pixel detector. And we employ differential HSI to suppress noise when calculating the spectrum. The coefficient $H(u, v)$ is calculated by differential computation [30-31].

Each pairs projection pattern of the differential HSI has two measurement values, one is obtained by projecting pattern $P_H(x, y)$ and the other is obtained by $1 - P_H(x, y)$, as shown in Fig. 2. The coefficient $H(u, v)$ is obtained by subtracting these two measurement values:

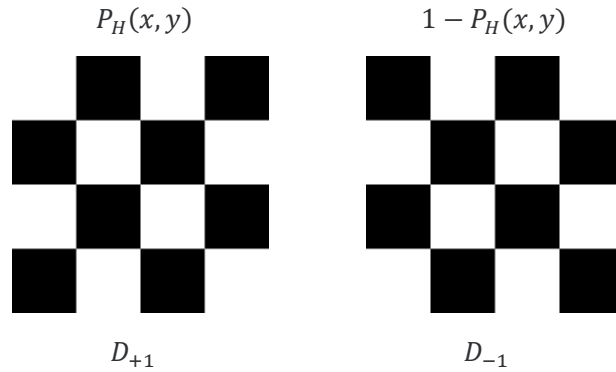


Fig. 2. Hadamard pattern.

$$H(u, v) = D_{+1} - D_{-1} \quad (2)$$

where D_{+1} and D_{-1} are the measurement values that correspond to $P_H(x, y)$ and $1 - P_H(x, y)$. Based on this, we can use Hadamard pattern projection curves and corresponding measurement coefficients to reconstruct the projection curve of the scene.

2.2. The first stage: Hadamard pattern sequence optimization method, EAHSI

In traditional computational ghost imaging (CGI), the quality of the image is determined by the number of patterns, which requires the large number of patterns to realize high imaging quality. However, the large number of measurements are time-consuming and are not suitable for fast and high-efficiency imaging. Recently, various algorithms have been developed to reduce the number of measurements [32-34], which have the advantages of few measurements, short imaging time, fast imaging speed and good imaging quality. Among them, CRHCGI [34] is superior to other methods.

The efficiency of pattern scanning single-pixel imaging technology depends on the degree of energy concentration of the image by using the transformation. If a transform can highly concentrate image energy in a band, that is, a small number of coefficients have large amplitude, it can simply measure these large-amplitude coefficients and ignore the rest to improve efficiency [24,33-34]. In light of this, a novel sampling method based on contour moment technology, named EAHSI, is utilized in the sampling phase of fast-moving objects detection and tracking to achieve an ultra-low sampling rate. Compared with CRHCGI [34], our method, which optimizes the projection order by the area size of the effective region, has better performance. The contour moment is used to calculate the area of the effective region in the pattern, and the white region shown in Fig. 1b is the effective region.

$$m_{ij} = \sum_{x,y} [Ctr(x,y) \cdot x^j \cdot y^i], i, j = 0,1. \quad (3)$$

The x, y represents the abscissa and ordinate of the points constituting the contour Ctr in the pattern of Fig. 3. Where m_{ij} is the result of the contour moment and when i, j is equal to 0, it means to calculate the contour area m_{00} .

The principle of the EAHSI: the larger the area of pattern effective region is, the more concentrated the image energy is [24,33-34]. As a result, the pattern, which can make the image energy highly concentrated, is preferentially selected to illuminate the object, and the rest is ignored. We reshape each row (or column) of the Hadamard matrix for getting the pattern. The size of the matrix is $128^2 \times 128^2$ in our work, part of which is illustrated in Fig. 1a. The maximum area of the effective region, which is reserved as the reference term to optimize the pattern sequence, is sorted in descending order.

Our method is applied to a 128×128 scene. A total of 16384 patterns are required when is full sampling. As shown in Fig. 3, the red box in Fig. 3a marks the effective region with the largest area in the pattern, Fig. 3b is the partial pattern sequence before optimization, Fig. 3c is the partial pattern sequence after optimization. The number indicates the specific position of the pattern in the sequence.

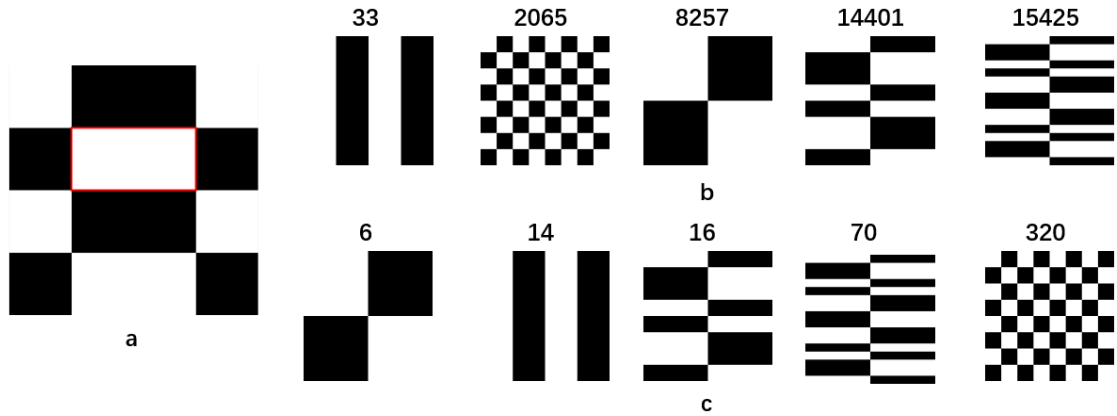


Fig. 3. The red box in 3a indicates the region with the largest effective area, the number in 3b is the position of patterns in the original sequence, and the number in 3c is the position of patterns in the optimized sequence.

As mentioned above, using the optimized sequence, we can collect the spectral information needed in the tracking stage through fewer measurement times for reconstructing the projection curves of the scene, in which the curves include position information of the fast-moving target. More details can be seen in the experiment part. Noted that the experimental imaging part is only to prove the advantage of the EAHSI, that is, implements an ultra-low sampling rate in the target detection and tracking stage.

2.3. The second stage: the non-imaging detection and tracking method, PCGD

We propose an image-free real-time detection and tracking method based on Hadamard single-pixel imaging theory. Using the HSI-based technology, we reconstruct the projection curves of a complex scene in the x-axis and y-axis direction, as shown in Fig. 4. And then we calculate the gradient difference of the projection curves to estimate the location of the fast-moving object. Inspired by the method of Shi et al. [20], the two-dimensional image is transformed into a one-dimensional projection curve, which greatly decreases the amount of calculation and storage space. We decompose the Hadamard pattern to measure the position information accurately and obtain more details when reconstructing the projection curve.

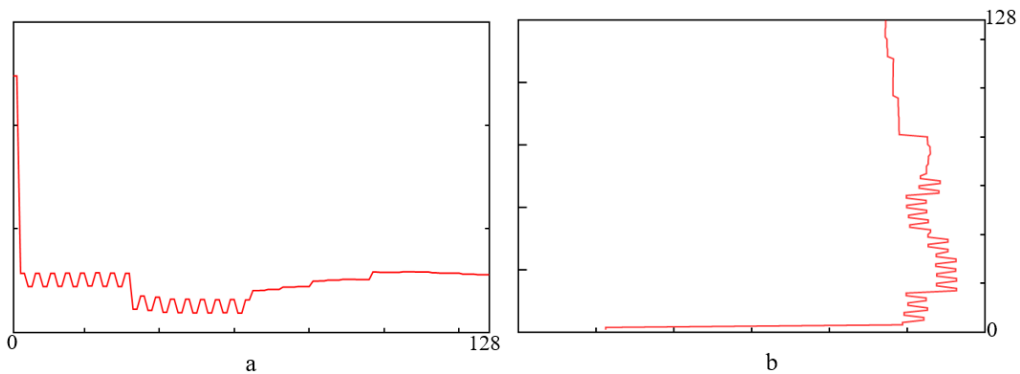


Fig. 4. The 4a and 4b respectively are the projection curves of the scene in the x-axis and y-axis directions at a certain frame.

To improve efficiency and enhance real-time performance, we use the pattern sequence optimized by the EAHSI, which dramatically reduces the number of measurements and enhances the detection and tracking speed. We decompose the pattern into rows and columns along the x-axis and y-axis for composing sub-pattern, as shown in Fig. 5. And the sub-pattern is projected

to illuminate the fast-moving target in the scene. We only use the sub-patterns that are not repeated in the same pattern.

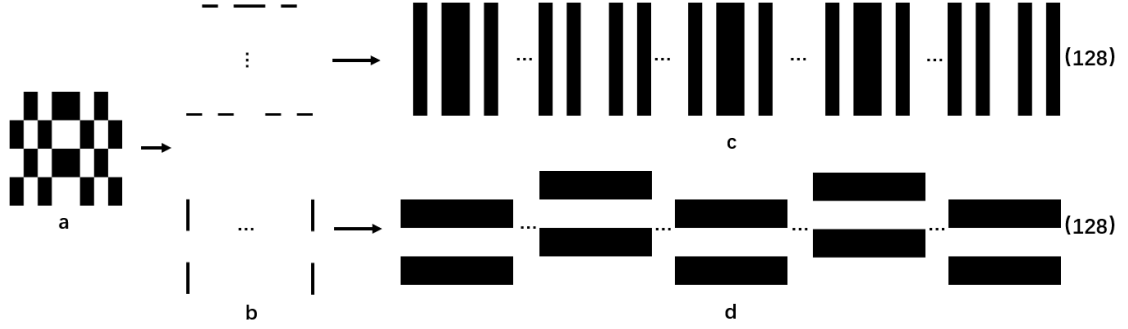


Fig. 5. The Hadamard basis pattern decomposition and the sub-patterns composition. 5a is the pattern of optimization sequence, 5b are the rows and columns decomposed from the pattern, 5c and 4d are the sub-patterns composed from the 5b.

In the whole process, it is not necessary to image the scene, but only need to apply the HSI principle to reconstruct the projection curve of the scene in the x-axis and y-axis direction. That is, to transform the two-dimensional information into one-dimensional information by projecting the sub-patterns. And, to reduce the amount of computation, we reconstruct prior projection curves and the first-order gradient of the projection curves for the scene before the fast-moving object enters. Furthermore, we use the gradient difference to estimate the location after the object enters the scene.

The step of using the PCGD to estimate the location is as follows: first, starting from the fast-moving object entering the scene, the HSI principle is used to reconstruct the projection curve along the x-axis and y-axis. The second step is to calculate the first-order gradient of the scene projection curve. The third step is to perform a gradient difference operation on the first-order gradient between the scene and the prior projection curve. The fourth step is to extract the first two maximum values of the gradient difference result to obtain the position information of the object in the scene. The interaction between sub-pattern and target scene is mathematically expressed as the internal product of both:

$$IP(P, I) = \sum_{x=1}^{128} \sum_{y=1}^{128} \text{abs}\{P(x, y)I(x, y)\} \quad (4)$$

where P represents the sub-pattern, I represents the scene, x and y are the coordinate values of the sub-pattern and the scene, and the single-pixel detector collects the measured value IP .

$$PC_x(m) = \sum_{x=1}^{128} P(x, m), m = 1, 2, \dots, 128. \quad (5)$$

$$PC_y(n) = \sum_{y=1}^{128} P(n, y), n = 1, 2, \dots, 128. \quad (6)$$

$$C(i) = PC(i), i = 1, 2, \dots, 128. \quad (7)$$

The PC_x and PC_y , a 1×128 vector, represents the projection of the P along with the x-axis and y-axis. The projection curve reconstructed from the projection of sub-patterns and the measured value can be expressed as Eq.8:

$$F(i) = IP(P, I) * C(i), i = 1, 2, \dots, 128. \quad (8)$$

where F is a 1×128 one-dimensional vector and represents the projection curve, as shown in the left of Fig. 10a, 10b and Fig. 11a, 11b. And then, we subtract the previous value from the next value in the one-dimensional vector for calculating the first-order gradient F' of F :

$$F'(i) = \nabla[F(i)] \quad (9)$$

$$F'_O(i) = \nabla[F_O(i)], \quad F'_M(i) = \nabla[F_M(i)] \quad (10)$$

the F'_O is the first-order gradient of the projection curve before the fast-moving object enter, call the prior projection curve. F'_M is the first-order gradient of the scene projection curve after the fast-moving object enter, as shown in the right of Fig. 10a, 10b and Fig. 11a, 11b.

$$Diff[m(i), n(i)] = abs[m(i) - n(i)], i = 1, 2, \dots, 128. \quad (11)$$

$$D(\nabla) = Diff(F'_O, F'_M) \quad (12)$$

The $Diff$ is the gradient difference operation and the $D(\nabla)$ is result. Finally, the position information of the target is obtained after the gradient difference operation, as shown in Fig. 10c and Fig. 11c.

$$(V_1, V_2) = S_2\{D(\nabla)\} \quad (13)$$

S_2 means to select the first two largest values.

As described previously, our method can estimate the boundary value of the target in the x-direction and y-direction in the scene. By continuously measuring the scene, we can get the location information of the target in consecutive frames. Finally, the proposed method implements fast-moving target detection and tracking in real-time without imaging. In a word, the proposed PCGD in this paper allows for the robust implementation of detecting and tracking and enables the ultra-low sampling rate capability by using the EAHSI.

3. Experiment results and analysis

3.1. Schematic diagram of the optical system

We demonstrate through experiments to prove that the PCGD and EAHSI methods are effective. As shown in Fig. 6, the illumination system consists of a white LED, a DMD (Texas Instruments DLP Discovery 4000 development kit), a single-pixel detector (Thorlabs DET100A2 320nm-1100nm), a data acquisition board (National Instruments USB-6343) and the projection lens.

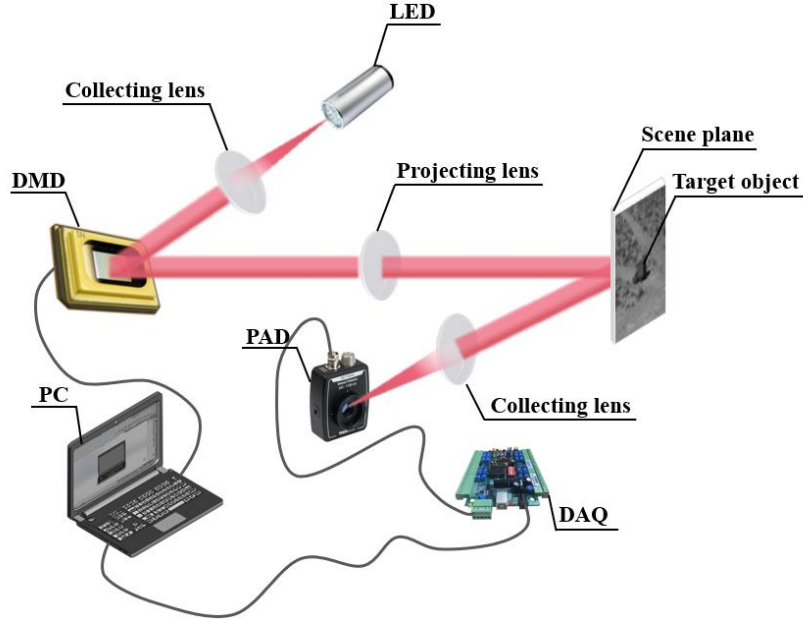
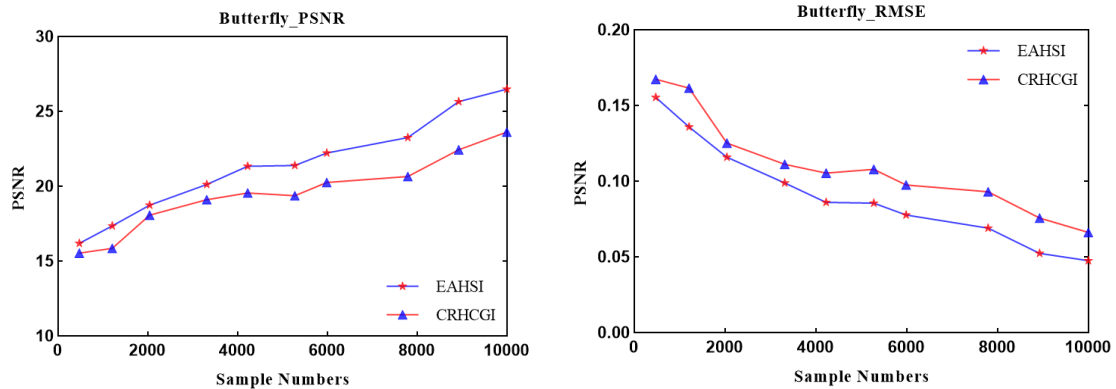


Fig. 6. Experimental set-up and Schematic diagram of the optical system.

In the illumination system, the DMD is illuminated by the LED, which has 2560×1600 micromirrors and the pixel size is $7.6\mu\text{m}$. And it is operated at a refresh rate of 22kHz . The Hadamard pattern, displayed on the DMD, is projected onto the scene through the lens. The single-pixel detector collects the light intensity, and the data acquisition board convert the light intensity signal into a digital signal.

3.2. Analysis of the EAHSI method

The experiment was divided into two stages. We first verify the effectiveness of EAHSI and then verify the tracking stage. Compared with the state-of-the-art methods, the ERHSI can reconstruct better results with fewer measurements. Without losing generality, we used both "Butterfly" and "Girl" images in the test. Fig. 8 shows the comparison between EAHSI and CRHCGI [34] when reconstructing, using the peak signal-to-noise ratio (PSNR) and the root mean squared error (RMSE) as the reference standard to evaluate image quality objectively. The larger the PSNR value, it indicates that the distortion between the image to be evaluated and the reference image is smaller, which is the image quality is better. And the smaller the value of RMSE, the better the image quality.



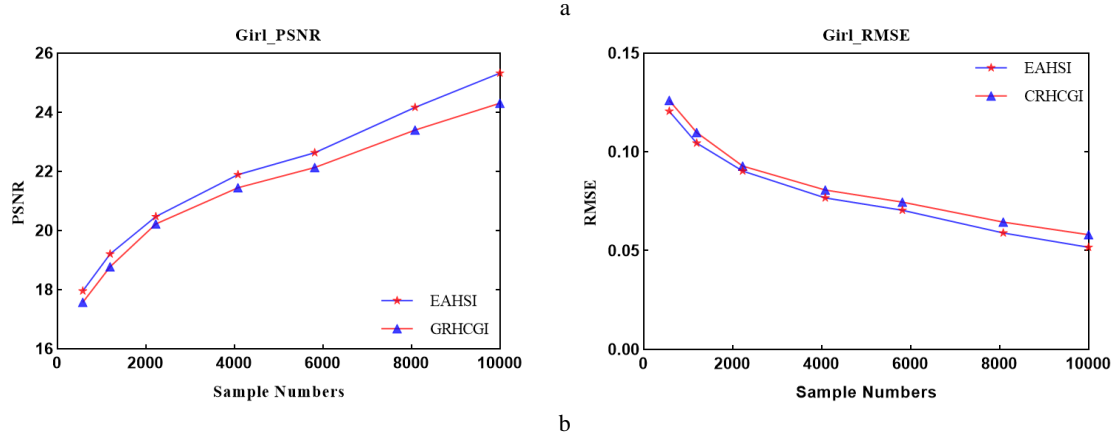


Fig. 7. The 7a and 7b are the PSNR curves and RMSE curves of Butterfly and Girl, respectively.

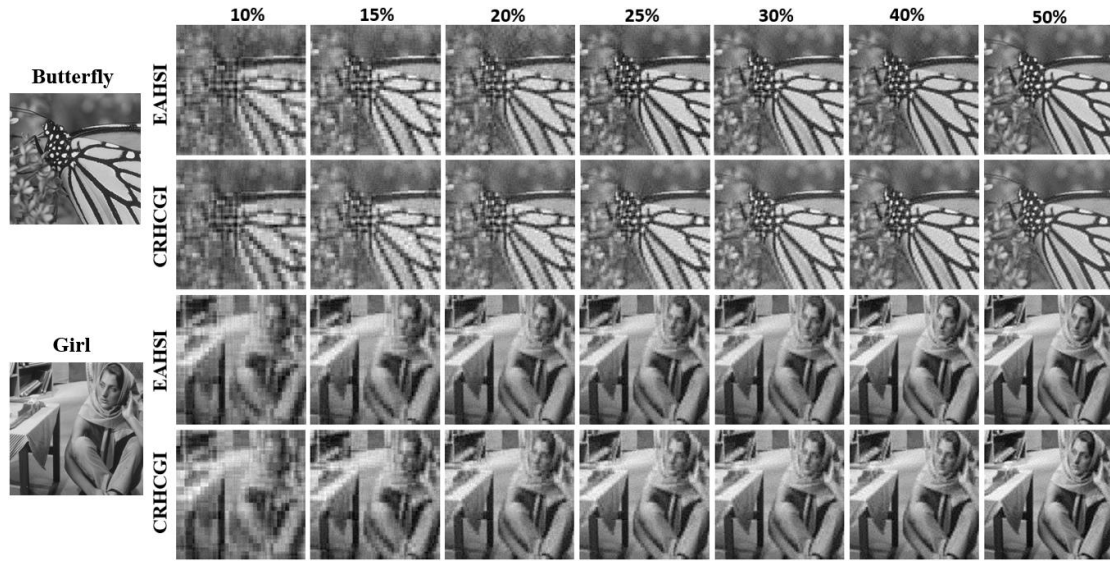


Fig. 8. Butterfly and Girl images reconstructed at different sampling rates.

It turns out to be the case that the PSNR of the EAHSI reconstruction image is higher than that of the CRHCGI under the same measurement times. Meanwhile, the measurement times of EAHSI is much less than that of CRHCGI under the same PSNR. Besides, the RMSE of EAHSI is lower than CRHCGI. Therefore, the efficiency of EAHSI is higher than that of CRHCGI under the condition of obtaining the same quality reconstruction results. Fig. 7 shows the reconstructed images at different sampling rates. From a subjective and objective standpoint, it is obvious that the EAHSI is better than CRHCGI.

3.3. Analysis of the detection and tracking method

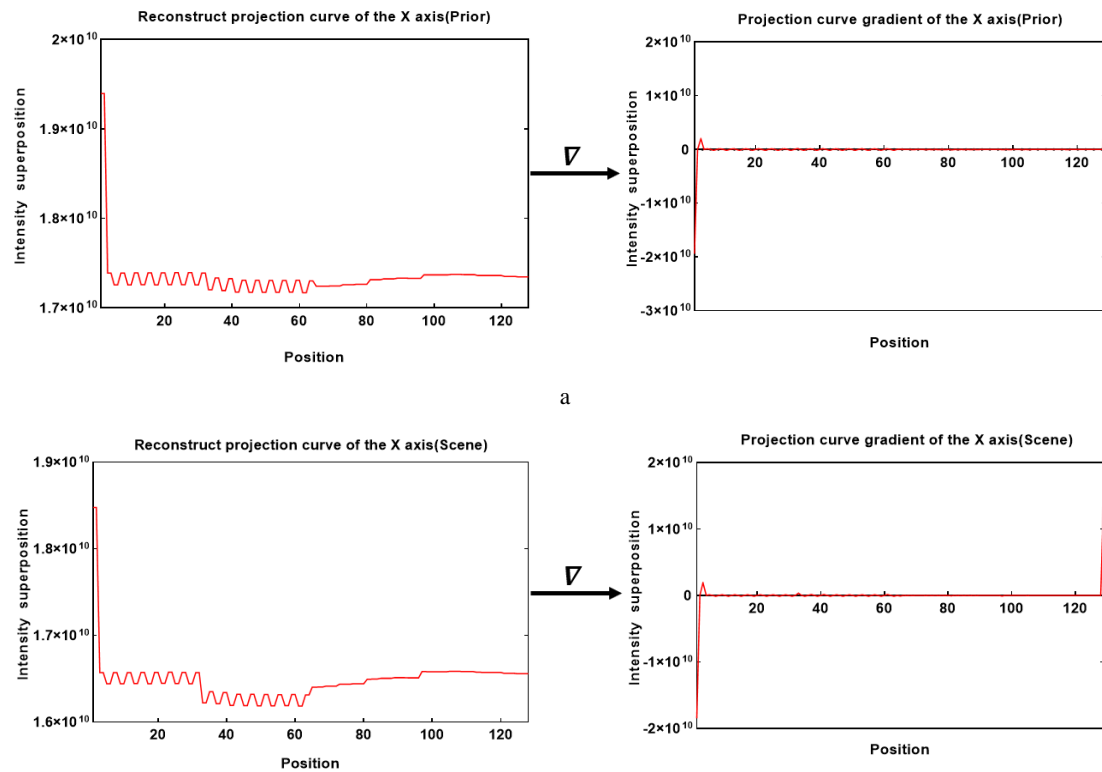
In the target detection and tracking stage, the Hadamard pattern sequence, optimized by EAHSI, is used for measuring the light intensity signal collected by the single-pixel detector. The sub-patterns are obtained by decomposing Hadamard pattern and projected by DMD. And then, based on the HSI principle, the projection curve of the sub-patterns and the collected measurement value are used to reconstruct the position information curve. Combining the prior curve, the PCGD method is further applied. Finally, the location information of the fast-moving object in the

complex scene is obtained.

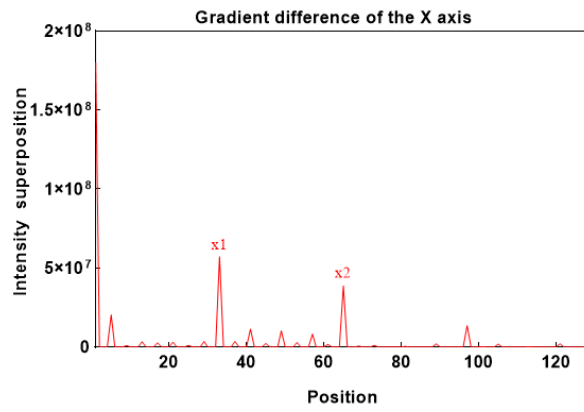
To describe the mechanism of the PCGD method in detail, we show the calculation of the position information of a fast-moving object in a certain transient state, the transient image as shown in Fig9. To facilitate observation and analysis, we place the y-axis projection curve graph horizontally, as shown in Fig.10 and Fig.11, which is different from the placement shown in Figure 4. The projection curve of the scene along the x-axis, shown on the left side of Fig. 10b, is reconstructed from the x-axis projection of the sub-pattern and the single-pixel measurement value. And the first-order gradient curve is calculated, as shown on the right side of Fig. 10b. The ∇ represents the gradient difference operation of a one-dimensional vector. Finally, perform a gradient difference operation on the first-order gradient curve of the scene and the prior first-order gradient curve shown in Fig. 10a to obtain the position information in the x-axis direction, as shown in Fig. 10c. In the same way, we can obtain the position information in the direction of the y-axis, as shown in Fig. 11c. Eventually, the position information of the fast-moving object at above transient can be estimated, that is, $(V_{1x}, V_{2x}) = (x1, x2)$, $(V_{1y}, V_{2y}) = (y1, y2)$.



Fig. 9. The fast-moving object in a certain frame.

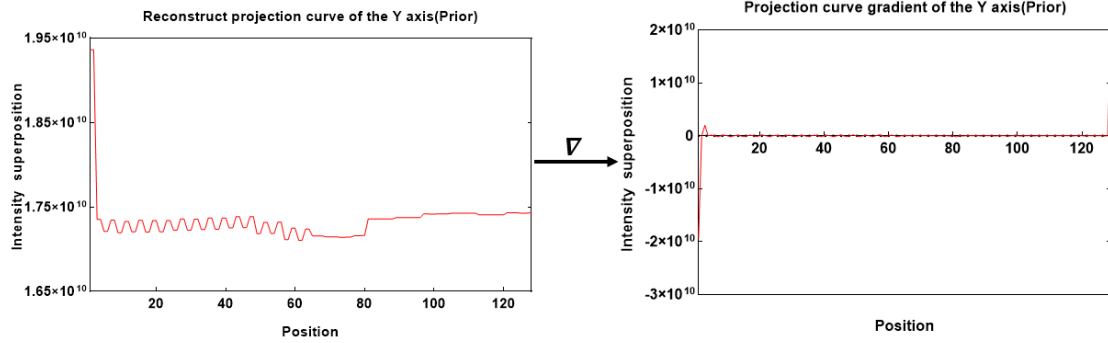


b

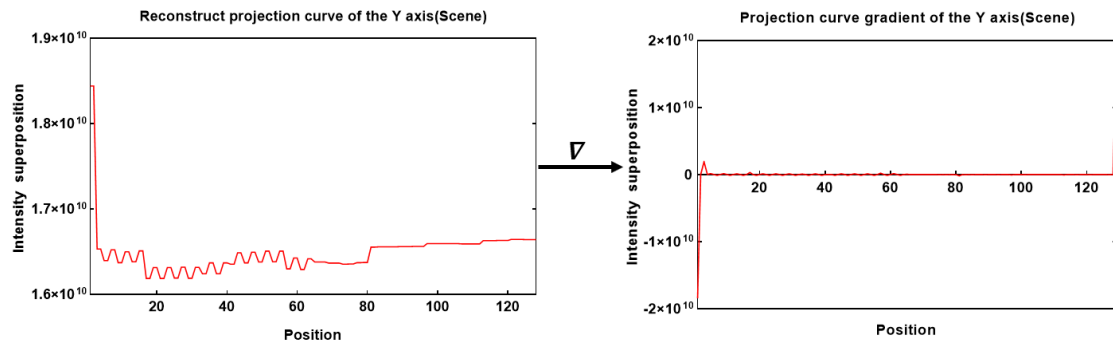


c

Fig. 10. The position information of the fast-moving object in the above transient state is calculated through the reconstructed projection curve of the x-axis direction.



a



b

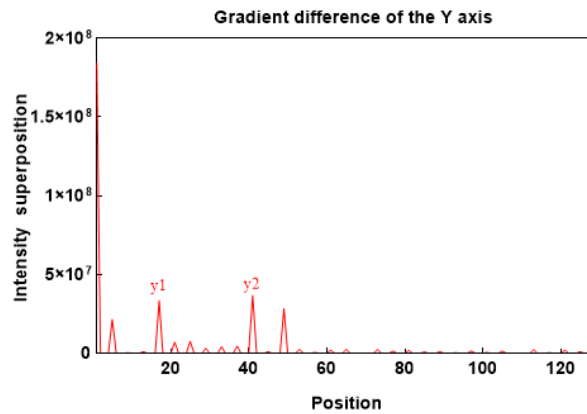
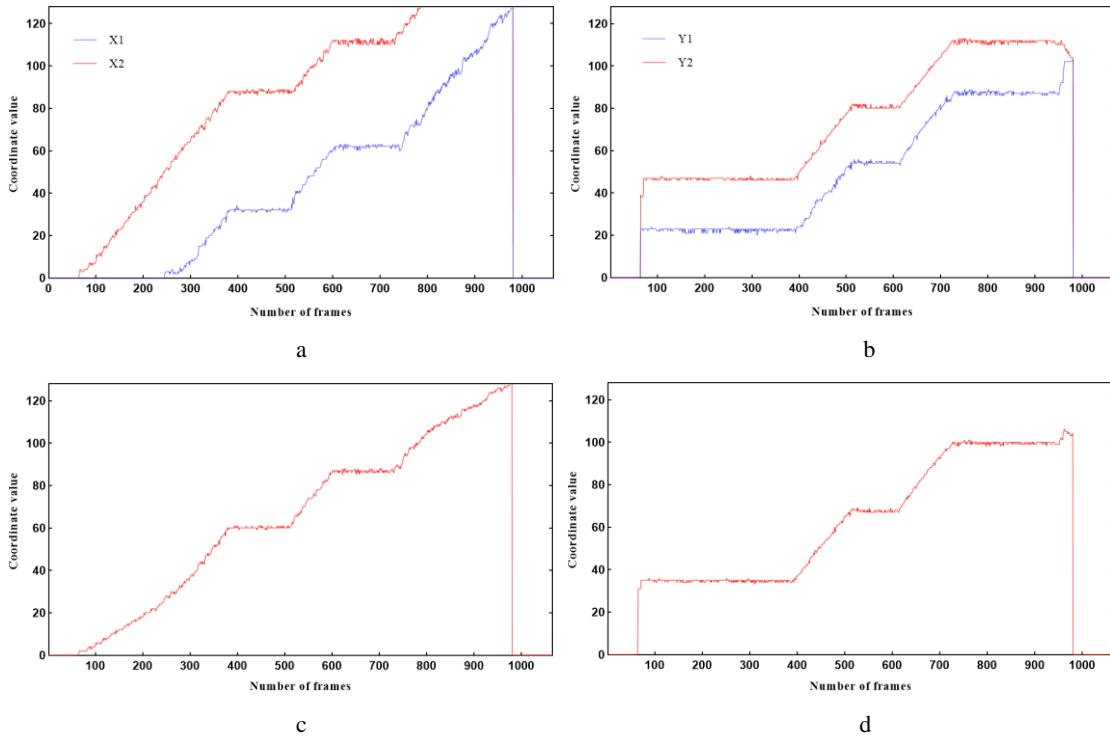


Fig. 11. The position information of the fast-moving object in the above transient state is calculated through the reconstructed projection curve of the y-axis direction.

During the experiment, the data acquisition board works at the maximum sampling rate, that is, 500000 data is sampled per second, which is far higher than the refresh rate of the DMD. Besides, we take ten single-pixel measurement values for each lighting mode, average them, and then reconstruct the projection curve. The gradient difference algorithm is employed to estimate the position information contained in the projection curve. Finally, we get the position information of the fast-moving object.

As shown in Fig.12, it represents the location information corresponding to different transient states of the object in the whole moving process. The horizontal axis represents the number of frames, and the vertical axis represents the coordinate values. Fig. 12a are the abscissas x_1 and x_2 of the object in the scene, and Fig. 12b are the ordinates y_1 and y_2 of the object. They are the boundary information of the target.

In the experiment, the system does not detect the boundary information before the target enters the scene. The two boundary values in the y-axis direction can be calculated at the same time when the object enters the scene. Meanwhile, the x-axis direction only detects x_2 . And the x_1 can be detected when the target fully enters the scene. When the x_2 value reaches its maximum value, it indicates that the target is leaving the scene. And the target is leaving the scene when all boundary values reach their maximum. We calculate the centroid of the fast-moving object in the scene through the boundary value when tracking the target. Figures 12c and 12d are the x and y coordinates of the centroid, respectively. Furthermore, we can get the motion trajectory of the fast-moving object, as shown in Fig. 12e.



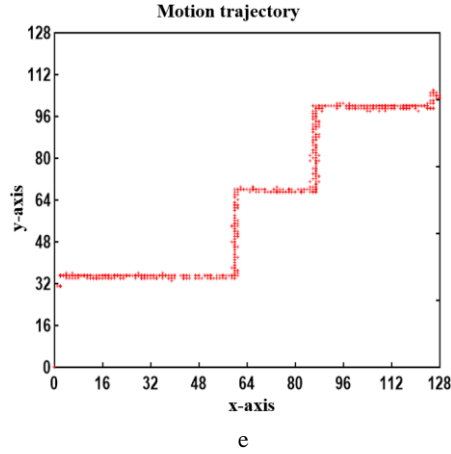


Fig. 12. The 12a-12d represent the position information of the fast-moving target at different transient states and 12e represents the motion trajectory.

Finally, our method achieves a 1.28% sampling rate, 0.00955s time resolution and 105 fps frame rate, which fully meets the requirements of real-time detection and tracking of fast-moving objects in complex scenes. In the calculation process, we need to obtain $128 \times 2 \times 3$ intermediate data, a total of 1024×3 bytes (about 2.9e-3MB), store 4 coordinate data, accounting for 16 bytes (about 2.45e-2MB) of location information, and the space occupied by the calculation is not more than 1MB.

Rich experiments prove the effectiveness of our method. It can obtain high-quality measurement values at an ultra-low sampling rate for estimating the object position information and has the ability for ultra-low time and space consumption. Compared with the state-of-the-art methods, our approach is not only capable of handling real-time tracking of an object in complex scenes, but it can estimate the boundary information of the object for performing segmentation and recognition.

3.4. Compared with the other detection and tracking method

As mentioned before, the detection and tracking methods in this article and [20] are both based on the HSI principle, but no imaging is required. In the sampling stage, reference [20] uses this optimization method, called "Russian dolls", that the principle is the transformation of the Hadamard matrix. The dimension of the matrix to be transformed will be larger when the size of the scene is large, which will increase the space-time overhead, and its performance is poor than CRHCGI. Our method makes use of contour moments to optimize the Hadamard pattern sequence. There is no large-dimensional matrix operation, and its performance is better than CRHCGI.

In the tracking stage, the method in [20] decomposes and reorganizes the Hadamard matrix. It combines the first-order derivative to detect the position information of the target. This detection method may have good results in a scene with a relatively simple background. And our approach decomposes and reorganizes the Hadamard pattern. The gradient difference operation is used to directly calculate the position information in the scene and without further operation. Finally, our method achieves 0.00304s time resolution and 329fps frame rate at a sampling rate of 0.41% when processing the scenes in [20], while the frame rate achieved by the method in [20] is about 177fps.

Furthermore, reference [21] is based on Fourier single-pixel imaging method to track the target. It employs 4 Fourier basis patterns to illuminate fast-moving objects. Its low sampling rate,

low time resolution, and high frame rate show that its performance is better than the method in [20] and this article. But it can only obtain the coordinate information of a certain point (centroid) on the object. While both in [20] and the method in this article can obtain the boundary information of the target, which can detect and segment the target to lay the foundation for subsequent recognition tasks.

In summary, our method can not only efficiently detect and track fast-moving targets in real-time but also segment fast-moving objects, laying a solid foundation for the next detection and recognition task of optical neural networks.

4. Discussion

We have studied and analyzed the impact of high-intensity values on imaging quality and found that the high-intensity values have a greater contribution to high-quality image reconstruction. The EAHSI-based methods can concentrate high-intensity values at the front of the pattern strength sequence. By comparing the experimental results of EAHSI and CRHCGI, we found that EAHSI can obtain higher quality imaging at lower sampling rates.

We have found that most object detection methods are mainly used for tangential moving. By analyzing the rules of axial moving. Our method also is suitable for the detection and tracking of axial moving. Combining two reference items to judge the object's moving type and the reference item can be expressed as:

$$\mathfrak{B}_x = \text{abs}(V_{1x} - V_{2x}) \quad \mathfrak{B}_y = \text{abs}(V_{1y} - V_{2y}) \quad (14)$$

if \mathfrak{B}_x and \mathfrak{B}_y change uniformly at the same time and the centroid is unchanged or changed slightly. It is judged to be an axial movement, and we will verify it in detail in future work.

We recognize the method proposed has three limitations: One is that it can only detect and track one fast-moving object at a time. The last one is that the proposed method can only achieve two-dimensional tracking. Breaking through the above limitations is our future work.

5. Conclusion

We have proposed a strategy including two stages for achieving fast-moving object detection and tracking in real-time. In the sampling stage, it exploited the EAHSI to reduce the number of measurements and improved the real-time performance of the system. And in the tracking stage, it used the PCGD to estimate the position information of the fast-moving object. Our strategy has implemented a 105fps frame rate at a 1.28% sampling rate when tracks. It is suitable for fast-moving object detection and tracking in real-time. This proposed method breaks through the traditional tracking ways, which can complete the segmentation task without prior knowledge of the target, providing a data source for the optical neural network recognition task.

Acknowledgments

This work is supported by NSFC under grants 61860206007 and U19A2071, as well as the funding from Sichuan University under grant 2020SCUNG205.

References

- [1] S. T. Park, J. G. Lee, An efficient filtering algorithm for improved radar tracking (1996).

- [2] Chaw.Bing, Chang, Tabaczynski, J., Application of state estimation to target tracking, *Automatic Control IEEE Transactions on* (1984).
- [3] F. Daum, R. Fitzgerald, Decoupled kalman filters for phased array radar tracking, *IEEE Transactions on Automatic Control* 28 (1984) 269–283.
- [4] S. T. Park, J. G. Lee, Improved kalman filter design for three-dimensional radar tracking, *IEEE Transactions on Aerospace and Electronic Systems* 37 (2001) 727–739.
- [5] M. S. Wei, F. Xing, Z. You, A real-time detection and positioning method for small and weak targets using a 1d morphology-based approach in 2d images, *Light: Science and Application (English version)* 7 (2018) 97–106.
- [6] D. Comaniciu, V. Ramesh, P. Meer, Kernel-based object tracking, *IEEE Transactions on Pattern Analysis and Machine Intelligence* 25 (2003) 564–577.
- [7] W. Zhong, H. Lu, M.-H. Yang, Robust object tracking via sparsity-based collaborative model, *IEEE Conference on Computer Vision and Pattern Recognition* (2012).
- [8] W. Gong, C. Zhao, H. Yu, M. Chen, W. Xu, S. Han, Three-dimensional ghost imaging lidar via sparsity constraint, *Scientific Reports* 6 (2016) 26133.
- [9] L. Hu, X. Jin, G. Zeng, Lensless ghost imaging for moving objects, *Optical Engineering* 50 (2011) 7005.
- [10] Z. H. Xu, W. Chen, P. José, P. Miles, M. J. Sun, 1000 fps computational ghost imaging using led-based structured illumination, *Optics Express* 26 (2018) 2427–2434.
- [11] F. Ferri, D. Magatti, L. A. Lugiato, A. Gatti, Differential ghost imaging, *Physical review letters* 104 (2010) 253603.
- [12] B. Sun, S. S. Welsh, M. P. Edgar, J. H. Shapiro, M. J. Padgett, Normalized ghost imaging, *Optics Express* 20 (2012) 16892–16901.
- [13] W. Gong, S. Han, A method to improve the visibility of ghost images obtained by thermal light, *Physics Letters A* 374 (2010) 1005–1008.
- [14] L. Bian, J. Suo, Q. Dai, C. Feng, Experimental comparison of single-pixel imaging algorithms, *Journal of the Optical Society of America A* 35 (2017) 78.
- [15] K. Guo, S. Jiang, G. Zheng, Multilayer fluorescence imaging on a single-pixel detector, *Biomedical Optics Express* 7 (2016) 2425.
- [16] E. Li, Z. Bo, M. Chen, W. Gong, S. Han, Ghost imaging of a moving target with an unknown constant speed, *Applied Physics Letters* 104 (2014) 251120–251120–3.
- [17] X. Li, C. Deng, M. Chen, W. Gong, S. Han, Ghost imaging for an axially moving target with an unknown constant speed, *Photonics Research* 3 (2015) 153.
- [18] S. Jiao, M. Sun, Y. Gao, T. Lei, Z. Xie, X. Yuan, Motion estimation and quality enhancement for a single image in dynamic single-pixel imaging, *Optics express* 27 (2019) 12841–12854.
- [19] Shuai, Sun, Jun-Hao, Hui-Zu, Lin, Liang, Jiang, Wei-Tao, Liu, Gradual ghost imaging of moving objects by tracking based on cross correlation., *Optics letters* 44 (2019) 5594–5597.
- [20] D. Shi, K. Yin, J. Huang, K. Yuan, W. Zhu, C. Xie, D. Liu, Y. Wang, Fast tracking of moving objects using single-pixel imaging, *Optics Communications* 440 (2019) 155–162.
- [21] Z. Zhang, X. Wang, G. Zheng, J. Zhong, Image-free real-time detection and tracking of fast moving object using a single-pixel detector., *Optics express* 27 (2019) 35394–35401.
- [22] M. P. Edgar, G. M. Gibson, M. J. Padgett, Principles and prospects for single-pixel imaging, *Nature Photonics* 13 (2019) 13–20.
- [23] Z. Zhang, X. Ma, J. Zhong, Single-pixel imaging by means of fourier spectrum acquisition,

- Nature Communications 6 (2014) 6225.
- [24] Z. Zhang, X. Wang, G. Zheng, J. Zhong, Hadamard single-pixel imaging versus fourier single-pixel imaging, *Optics Express* 25 (2017) 19619–19639.
- [25] Z. Zhang, S. Liu, J. Peng, M. Yao, G. Zheng, J. Zhong, Simultaneous spatial, spectral, and 3d compressive imaging via efficient fourier single-pixel measurements, *Optica* 5 (2018) 315–319.
- [26] M. Sun, M. P. Edgar, G. M. Gibson, B. Sun, N. Radwell, R. Lamb, M. J. Padgett, Single-pixel three-dimensional imaging with time-based depth resolution, *Nature Communications* 7 (2016) 12010.
- [27] W. K. Pratt, J. Kane, H. C. Andrews, Hadamard transform image coding, *Proceedings of the IEEE* 57 (1969) 58–68.
- [28] Decker, Jr, A. J., Hadamard-transform image scanning, *Applied Optics* 9 (1970) 1392–1395.
- [29] J. Gourlay, P. Mcowan, D. G. Vass, I. Underwood, M. Worboys, Time-multiplexed optical hadamard image transforms with ferroelectric-liquid-crystal-over-silicon spatial light modulators, *Optics Letters* 18 (1993) 1745–7.
- [30] C. M. Watts, D. Shrekenhamer, J. Montoya, G. Lipworth, J. Hunt, T. Sleasman, S. Krishna, D. R. Smith, W. J. Padilla, Terahertz compressive imaging with metamaterial spatial light modulators, *Nature Photonics* 8 (2014) 605–609.
- [31] M.-J. Sun, M. P. Edgar, D. B. Phillips, G. M. Gibson, M. J. Padgett, Improving the signal-to-noise ratio of single-pixel imaging using digital microscanning, *Optics Express* 24 (2016) 10476–10485.
- [32] X. Yu, R. I. Stantchev, F. Yang, E. Pickwell-MacPherson, Super sub-nyquist singlepixel imaging by total variation ascending ordering of the hadamard basis, *Scientific Reports* 10 (2020) 9338.
- [33] M.-J. Sun, L.-T. Meng, M. P. Edgar, M. J. Padgett, N. Radwell, A russian dolls ordering of the hadamard basis for compressive single-pixel imaging, *Scientific Reports* 7 (2017) 3464.
- [34] H. Wu, G. Zhao, R. Wang, H. Xiao, D. Wang, J. Liang, L. Cheng, R. Liang, Computational ghost imaging system with 4-connected-region-optimized Hadamard pattern sequence, *Optics and Lasers in Engineering* 132 (2020) 106105.